J. Biochem. 129, 163–171 (2001)

Geometric Effect of Matrix upon Cell Differentiation: BMP-Induced Osteogenesis Using a New Bioglass with a Feasible Structure[1]

Javed Mahmood,* Hiroko Takita,* Yasutaka Ojima,* Masahiro Kobayashi,† Takao Kohgo,‡ and Yoshinori Kuboki*,[2]

*Department of Oral Health Science and ‡Department of Oral Pathobiology, Graduate School of Dentistry, Hokkaido University, N-13, W-7, Kita-ku, Sapporo 060-8586; and †Chiba Institute of Technology, 17-1, Tsudanuma, 2-chome, Narashino, Chiba 275

Received August 28, 2000; accepted November 6, 2000

A new biocompatible glass, which is composed of CaO, P_2O_5, SiO_2, and Al_2O_3 (abbreviated CPSA) and is characterized by higher elasticity than previous bioglass products, was molded into fibers with a diameter of 9 μm. With CPSA fibers, two geometrically different structures, balls and bundles (each 20 mg in weight), were prepared, combined with 2.2 μg of rhBMP-2 (a gift from Yamanouchi Co., Japan) and implanted subcutaneously into rats. The histology showed remarkably higher bone formation in the ball-CPSA/BMP at 2 and 4 weeks than in the bundle-CPSA/BMP. The ball-CPSA/BMP showed 10 times higher alkaline phosphatase (ALP) activity at the second week and 5 times higher osteocalcin content at the fourth week than the bundle-CSPA/BMP. Vascular development in the implants was evaluated by mRNA expression of Flt-1 and KDR, two receptors for vascular endothelial growth factor (VEGF). Both receptors showed higher expression in the case of the ball, while they were not detected in the bundle. It is concluded that the BMP-induced bone formation depends highly upon the porous vasculature-inducing geometry of the matrix, which can be constructed with the new CPSA fibers.

Key words: bone morphogenetic protein, bioglass, carrier-geometry, osteogenesis, vascularization.

To clarify the biochemical mechanism of bone formation and to formulate a tissue engineering strategy for bone tissue, we have proposed that five factors must be taken into consideration (*1–4*). These are (i) the cells involved directly in bone formation, (ii) matrices produced by the cells, (iii) body fluid provided by vascularization, (iv) regulators of general cellular activities as well as the calcification process, and (v) mechanical stress. These five factors should be analyzed individually, after which the interactions among them can be elucidated (*4–6*), and finally they should be integrated into the whole picture of bone formation. The principle can be applied not only to understanding the mechanism of bone formation but also to reconstructing local bone defects by tissue engineering (*2, 7–11*).

To verify the above proposition, we chose as our experimental system BMP-induced ectopic osteogenesis (*11, 12*). In this system, body fluid and some mechanical stress are already available in the local area, if it is in the right place at the right time. The only items that must usually be added are the regulators and matrices, which correspond to BMP and its carrier, respectively. BMP is a cytokine that was originally known for its unique character of inducing bone formation when implanted with a certain carrier into ectopic tissues such as skin or muscle (*13, 14*). This characteristic has naturally attracted the strong attention of scientists in the orthopedic and dental fields, in anticipation of its clinical application. One of the major problems to be overcome before clinical application is now considered to be the development of the optimal carrier of this cytokine (*11*).

Thus, we have developed and tested more than ten different carriers, coming to the conclusion that BMP-induced osteo- and chondrogenesis are highly dependent upon the carrier (*11, 15*). This is partly because the carrier of BMP functions not only as a mere drug delivery system, but also as an important cell substratum on which the cells undergo growth and differentiation (*11, 15*). At the initial stage of research, BMP-induced bone formation was believed to follow endochondral ossification precisely (*12*). However, when new carriers of porous particles of hydroxyapatite (PPHAP) or fibrous collagen membrane were introduced, it was found that bone was formed directly following the process of membranous ossification, without any detectable amount of cartilage formation (*15, 16*). Furthermore, the nonporous particles of hydroxyapatite did not induce bone or cartilage (*11*). These findings led us to investigate the geometry of the BMP carrier as one of the important factors that control the efficacy of the phenotype induction in this experimental system. A series of studies revealed that there are "cartilage-inducing carriers," such as a fibrous glass membrane (*15*), and "bone-inducing carriers," such as

[1]This study was supported in part by Grants-in-Aid (Nos. 04557078, 05454495, 06557095, 07457437, and 08557096) from the Ministry of Education, Science, Sports and Culture of Japan.

[2]To whom correspondence should be addressed. Phone: +81-11-706-4231, Fax: +81-11-706-4877, E-mail: kuboki@den.hokudai.ac.jp

Abbreviations: ALP, alkaline phophatase; BMP, bone morphogenetic protein; Flt-1, fms like tyrosine kinase 1; KDR, kinase domain region; VEGF, vascular endothelial growth factor.

PPHAP (*15*) and titanium fiber mesh (*17*).

In 1997, we found that the optimal pore size of porous blocks of hydroxyapatite (PBHAP) as a carrier of BMP to induce direct bone formation is 300–400 μm (*3*). Detailed comparison was done among PBHAPs with a series of pore sizes from 100 to 600 μm to examine their bone-inducing efficacies by determining alkaline phosphatase activities and osteocalcin contents. Both parameters of bone formation had the highest values in PBHAP implants with a pore size of 300–400 μm combined with rhBMP-2 (*3*).

To verify the "vasculature-inducing geometry hypothesis," fibrous types may also be useful BMP-carriers, obviously because collagen fibrils are the essential framework of the connective tissues. Biomimetic fibrous materials, constructed of quartz glass (CaO, SiO_2, BO_4, Al_2O_3) with a diameter of 1 μm and pore size of 1 μm, as determined by the maximum particle size that can get through, have already been tested as BMP-carriers and shown to induce cartilage exclusively within the fibrous structure of the membrane form (*18*). But a fibrous structure with a larger pore size is not available with the same quartz glass, mainly due to the fragility of the material.

In this paper, we chose CPSA as a BMP carrier, since this glass has sufficient rigidity while at the same time is elastic enough to be molded into fibers of reasonable strength (*19, 20*). With this CPSA, we prepared two geometrically different structures, balls and bundles (each 20 mg in weight), combined them with rhBMP-2, and implanted them into rats.

MATERIALS AND METHODS

Preparation of CPSA Glass—The components of CPSA glass (CaO: 32.24, P_2O_5: 9.26, SiO_2: 41.00, Al_2O_3: 17.50 mol%) were mixed, ground and melted at 1,400–1,450°C in a crucible. A nozzle 3.2 mm in diameter at the bottom of the crucible was opened and the melted glass was led vertically to form a fiber 2 meters in length. The end of the fiber was wound on a wheel at a speed of 700–1,000 m/min. The diameter of the final glass fiber (8–30 μm) could be controlled by the speed of rotation of the wheel. The tensile strength and modulus of elasticity of the CPSA fibers were about 2,100 MPa and 69.0 GPa, respectively.

Preparation of BMP-Carrier Composite—The CPSA glass fiber (9 μm in diameter) was cut into small pieces about 2–3 mm in length. These pieces were then molded manually into a ball 6–7 mm in diameter. This preparation was designated ball-CPSA. On the other hand, CPSA fibers were cut into pieces 7 mm in length, and these pieces were gathered into bundles 3 mm in diameter and bound with nylon strings. This preparation was designated bundle-CPSA. Both preparations weighed 20 mg. The ball- and bundle-CPSA were each infused with a solution (2.2 μg/30 μl) of rhBMP-2 (a gift from Yamanouchi Co., Japan).

Implantation—Male Wistar rats (about 70 g) were anesthetized intraperitoneally with pentobarbital sodium (4 mg/100 g body weight). The back was shaved, and cleaned with 70% alcohol and cut by blunt dissection to form subcutaneous pockets. Balls and bundles of CPSA glass fibers were implanted carefully with tweezers in the subcutaneous pockets and sutured. The animals were killed by an overdose of ether 1, 2, 3, 4, 8, or 20 weeks after implantation. The implants and the surrounding tissues that formed clearly discrete pellets were removed and subjected to histological observation and biochemical analysis.

Histological Observation—A part of each implant was fixed in 10% buffered formalin, decalcified with 40% formic acid, processed for paraffin embedding and cut into sections 5 μm thick. Sections were stained with hematoxylin-eosin and evaluated by light microscopy. One-week samples of ball-CPSA/BMP were also stained with toluidine blue.

Biochemical Analysis—Alkaline Phosphatase (ALP) Activity—The implanted pellets were lyophilied and stored at −80°C until use. Samples were cut with scissors in conical microcentrifuge tubes into a fine powder with a particle size of about 0.1 mm and mixed in 1 ml of 0.2% Nonidet P-40, 10 mM Tris-HCl, 1 mM $MgCl_2$, pH 7.5. The ALP activity of the suspension was measured by the Kind-King phenylphosphate method (*21*).

Osteocalcin Content—Pulverized samples were decalcified with 40% formic acid at 4°C for 12 h, keeping the pH constant at 2.0 by the addition of 40% formic acid. The decalcified solution was collected by centrifugation at 10,000 ×*g* for 30 min. The supernatant was dialyzed against distilled water and lyophilized. The samples were dissolved in phosphate-buffered saline (PBS) for sandwich ELISA. Rat osteocalcin and rabbit anti–rat osteocalcin affinity purified polyclonal antibody were used as standards for osteocalcin and the first antibody, respectively (a kind gift from Dr. Y. Dohi, Nara Medical University). A monoclonal anti-osteocalcin antibody (Takara, Japan) and goat anti–mouse IgG-HRP (Horse radish peroxidase), (Kirkegaard and Perry Laboratories, USA) were also used. For the substrate solution, ABTS (2,2′-azino-bis[3-ethylbenzothiazoline-6-sulfonic acid]diammonium salt) was used (Boehringer Mannheim GmbH, Germany).

The polyclonal anti–rat osteocalcin antibody was diluted 300-fold with PBS, added to a Falcon 96-well microtiter plate, and incubated overnight at 4°C. On the second day, the antibody was aspirated and 1% BSA (Bovine serum albumin)–TBS (0.05 M Tris-HCl/0.1 M NaCl, pH 8) was added as blocking solution and incubated for two hours at 37°C, then aspirated and washed with PBS three times. Standard osteocalcin antigen was diluted with PBS/15 mM EDTA at 1, 10, 50, 100, 250, or 500 ng/ml and added to the wells. Samples were diluted with PBS/15 mM EDTA, and also added to the wells and incubated at 37°C for 4 h, then aspirated and washed three times with 0.05% Tween 20/TBS (TTBS). The monoclonal anti-osteocalcin antibody (diluted 2,000-fold with 1% BSA-TBS) was added to the wells and the mixtures were incubated at 37°C for two hours. The antibody solution was aspirated, and wells were washed three times with TTBS. Anti–mouse IgG-HRP (horse radish peroxidase, diluted 1,000-fold with 1% BSA–TBS) was added and the mixtures were incubated at 37°C for 2 h. The antibody was aspirated and the wells were washed three time with TTBS. ABTS substrate (ABTS powder/0.1 M citric acid/0.2 M NaH_2PO_4/30% H_2O_2) solution was added and a greenish blue color appeared after 5–10 min, after which the reaction was stopped with 0.1 M citrate/0.1% NaN_3 solution. The absorbance was measured at 415 nm using a microtiter plate reader. The osteocalcin contents of the samples were calculated from the standard curve.

RNA Extraction and RT-PCR—For mRNA Expression of Osteocalcin, Flt-1, and KDR—Sample RNA was extracted

with Isogen reagent (Nippon Gene, Japan) according to the manufacturer's instructions. Briefly, fresh explanted pellets were homogenized and solubilized in an Isogen/chloroform solution at 4°C. Supernatants were obtained by centrifugation at 12,000 ×*g* for 15 min at 4°C and combined with isopropanol, after which the mixtures were centrifuged at 12,000 ×*g* for 15 min at 4°C. The precipitates were obtained by decantation and washed with 75% ethanol. Finally, the RNA pellets were dissolved in RNAase-free water and preserved at −20°C until used.

Using the extracted RNA as a template, reverse transcription reactions were carried out with an RNA-PCR Kit (Takara Biomedicals, Japan) to synthesize cDNA. Then, PCR was carried out using osteocalcin and GAPDH (a housekeeping gene) primers. The sequences of the osteocalcin primers were: 5′-ATGAGAGCCCTCACACTCCTC-3′ (sense) and 5′-CTAGACCGGGCCGTAGAAGCG-3′ (antisense) (*22*). The product size was 303 bp. PCR amplification was performed for 28 cycles in a thermocycler (Takara PCR, Thermal Cycler Personal, Takara Biomedicals) with initial denaturation at 95°C for 30 s. Subsequent annealing was done at 62°C for 30 s, and extension at 72°C for 1.5 min.

For the Flt-1 and KDR mRNA expression study, PCR was carried out using Flt-1 and KDR primers. The sequences of the rat Flt-1 primers were 5′- AAGGTCTACAGCACCAAG-3′ (sense; corresponding to nt 3220–3237) and 5′-CACATCATCAGAGCTTCC-3′) (antisense; corresponding to nt 3616–3633). The product size was 410 bp. The KDR primers were 5′-GGGAAAGACTATGTTGGG-3′ (sense; corresponding to nt 2830–2847) and 5′-ATCAATCTTGACCCCAGG-3′ (antisense corresponding to nt 3307–3324) (*23*). The product size was 490 bp. PCR amplification was performed for 35 cycles in a thermocycler (Takara PCR, Thermal Cycler, Takara Biomedicals) for both Flt-1 and KDR primers, with initial denaturation at 94°C for 1 min, subsequent annealing at 50°C for 1 min, and extension at 72°C for 10 min. Then, all the PCR products (Osteocalcin, Flt-1, KDR, and GAPDH) were analyzed by electrophoresis in 2% agarose gels, and stained with ethidium bromide.

RESULTS

Histological Changes—Figure 1 shows photographs of ball- and bundle-CPSA before implanting. Figure 2, A and B, shows the scanning electron microscopy profiles. The ball-CPSA has a higher porosity than the bundle-CPSA. By simple calculation, the roughly spherical ball-CPSA with a diameter of 6 mm comprising 20 mg of fibers with a fiber diameter of 9 μm and length of 3 mm, possesses approximately 3 times more vacant space than the bundle-CPSA

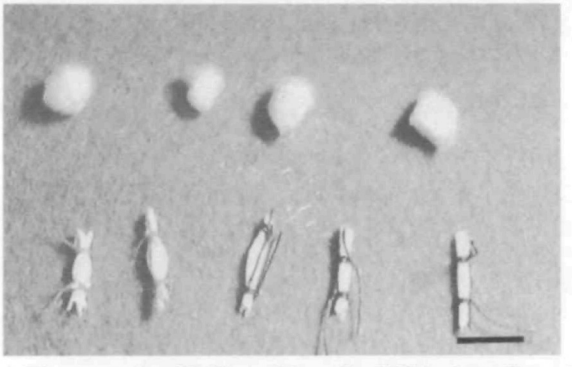

Fig. 1. **Photograph of ball- and bundle-CPSA glass fibers before implantation.** The a bar in the lower right corner indicates 5 mm.

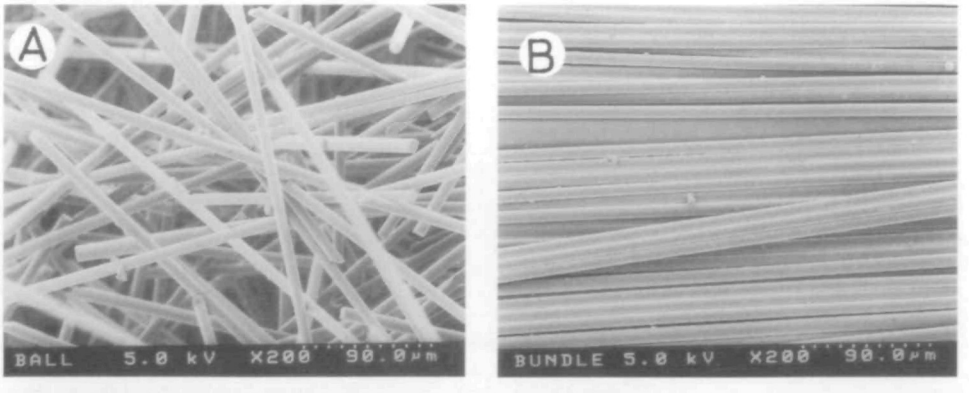

Fig. 2. **Scanning electron microscopic photograph of ball-CPSA (A) and bundle-CPSA (B) implants before implantation.**

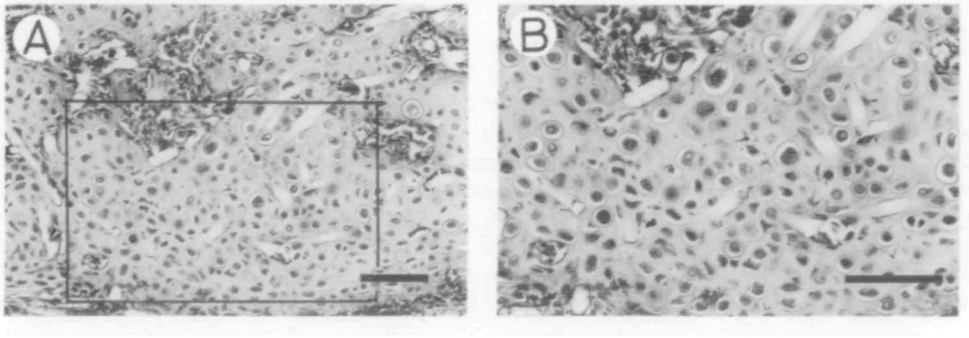

Fig. 3. **Microphotograph of cross-sections of ball-CPSA/BMP at 1 week after implantation.** A, Ball-CPSA combined with rhBMP-2. Hypertrophic chondrocytes are indicated by the box and shown enlarged in B. Large areas of chondrogenesis are observed. Sections were stained with toluidine blue. The bars in the lower right corners indicate 100 μm.

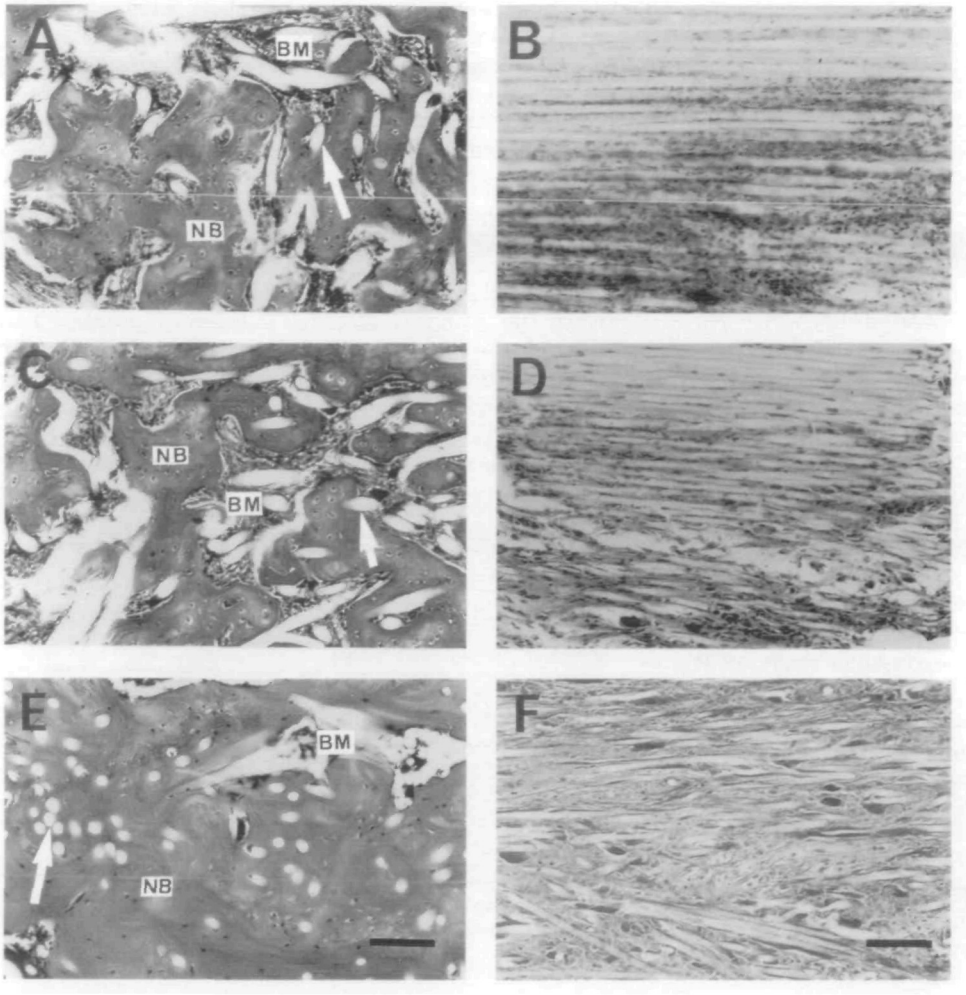

Fig. 4. **Microphotographs of CPSA-balls and bundles combined with rhBMP-2 at 2 weeks after implantation.** Much higher bone and marrow formation in ball-CPSA/BMP (A) than in bundle-CPSA/BMP implants (B). Bone and marrow formation are indicated by NB and BM, respectively. At 4 weeks after implantation, the ball-CPSA/BMP shows a large amounts of bone and marrow formation (C), whereas bundle-CPSA/BMP shows scant bone formation (D). At 20 weeks after implantation, lamellar bone formation with a widening of the bone marrow spaces is observed in ball-CPSA/BMP (E). In ball-CPSA without rhBMP-2 at 4 weeks time, neither bone nor cartilage is observed (F). Sections were stained with hematoxylin-eosin. Arrows indicate the CPSA glass fibers. The bars in the lower right corners indicate 100 μm.

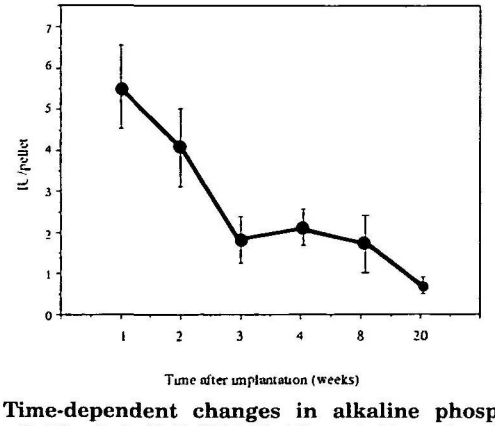

Fig. 5. **Time-dependent changes in alkaline phosphatase (ALP) activities in ball-CPSA/BMP from 1–20 weeks after implantation.** Vertical bars indicate standard deviations (n = 4).

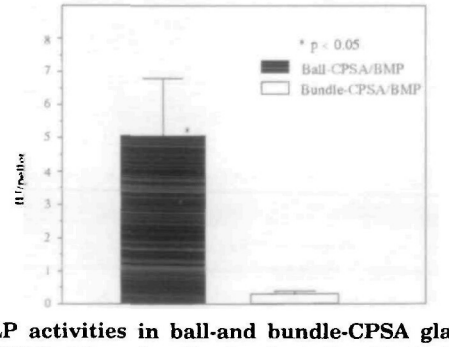

Fig. 6. **ALP activities in ball-and bundle-CPSA glass fibers with rhBMP-2 at 2 weeks after implantation.** Vertical bars indicate standard deviations (n = 3). Values significantly different from the bundle-CPSA/BMP are marked: $^*p < 0.05$, as determined by paired t-test analysis.

with a diameter of 3 mm, comprising 20 mg of fiber with a diameter of 9 μm and length of 7 mm.

Figure 3 shows the histology of the ball-CPSA/BMP at the first week. Numerous characteristic chondrocytes with some hypertrophic chondrocytes are already observed, indicating active chondrogenesis and differentiation in the ball-CPSA. At the same period, some areas show the transition stage from cartilage to bone. At the second week, newly formed bone all around the implant, and bone marrow formation between the CPSA fibers, are observed as shown in Fig. 4A. In contrast, bundle-CPSA/BMP at the second week show fibrous tissues around the implant, with only scanty bone formation as shown in Fig. 4B. There was also no detectable formation of cartilage in the bundle-CPSA/BMP implants (Fig. 4B). At 4 weeks, the ball-CPSA/BMP shows

increased amounts of new bone and bone marrow increased around the implant material as shown in Fig. 4C, whereas only scant bone formation can be seen in the bundle-CPSA/BMP (Fig. 4D).

The induced ectopic bone in the ball-CPSA continued active remodeling up to at least week 20 after implantation. Figure 4E shows abundant lamellar bone formation with widening of the bone marrow spaces at the twentieth week in the ball-CPSA/BMP. No inflammatory reaction was detected throughout the observation period. However, without rhBMP-2, the ball-CPSA generated neither bone nor cartilage formation, as exemplified by the picture at the fourth week shown in Fig. 4F, where only fibrous connective tissue can be seen.

Changes in Alkaline Phosphatase Activity—The time-dependent changes in the alkaline phosphatase activity (ALP) of the ball-CPSA/BMP from 1 to 20 weeks showed the highest ALP activity at 1 week, with a gradual decrease thereafter (Fig. 5). The ALP activity of the ball- CPSA/BMP at the second week was 10 times higher ($^*p < 0.05$) than that of the bundle-CPSA/BMP (Fig. 6).

Expression of mRNA for Osteocalcin—Figure 7 shows the agarose gel electrophoresis pattern of mRNA expression using RT-PCR. Lane 1 is the standard. Osteocalcin bands were detected in lanes 2, 4, 6, 8, 10, and 12, which represent, 1-, 2-, 3-, 4-, 8-, and 20-week samples, respectively, of ball-CPSA/BMP at the 303 bp region. Lanes 3, 5, 7, 9, 11, and 13 show GAPDH expression at 1, 2, 3, 4, 8, and 20 weeks, respectively. The GAPDH bands were observed in the 343 bp region.

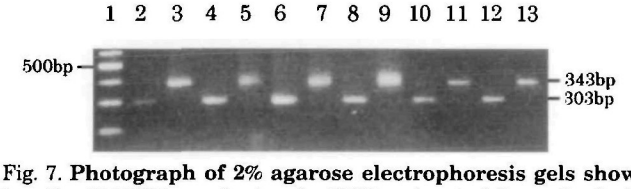

Fig. 7. **Photograph of 2% agarose electrophoresis gels showing the RT-PCR products of mRNA extracted from the ball-CPSA/BMP at 1, 2, 3, 4, 8, and 20 weeks after implantation and stained with ethidium bromide.** The GAPDH bands appear in lanes 3, 5, 7, 9, 11, and 13 at the 343 bp site. The bands at the 303 bp site are osteocalcin in 1, 2, 3, 4, 8, and 20 week samples in lanes 2, 4, 6, 8, 10, and 12, respectively. The first lane on the left is a 100-bp marker ladder.

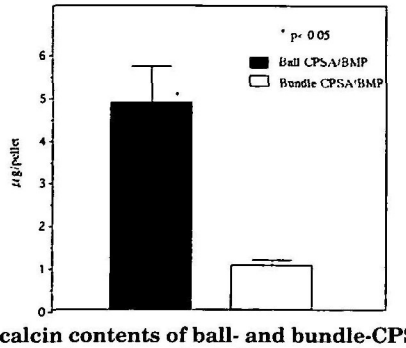

Fig. 8. **Osteocalcin contents of ball- and bundle-CPSA/BMP at 4 weeks after implantation.** Vertical bars indicate standard deviations ($n = 3$). Values significantly different from that of the bundle-CPSA/BMP are marked: $^*p < 0.05$, as determined by paired t-test analysis.

Changes in Osteocalcin Content—Figure 8 shows the osteocalcin contents of ball- and bundle-CPSA/BMP at 4 weeks after implantation, as measured by the sandwich ELISA technique. Ball-CPSA combined with rhBMP-2 had an osteocalcin content 5 times higher than the bundle-CPSA /BMP implants ($^*p < 0.05$).

Expression of Flt-1 and KDR—Figure 9 shows the 2% agarose gel electrophoretic pattern of mRNA expression of both ball- and bundle-CPSA combined with rhBMP-2 at 2 weeks, using GAPDH, Flt-1 and KDR primers. Lane 1 is the standard. GAPDH (as a control) expression was detected as a band corresponding to 343 bp in both ball- and bundle-CPSA/BMP in lanes 2 and 3, respectively. The ball-CPSA/BMP implants showed Flt-1 and KDR expression detected as bands at 410 and 490 bp in lanes 4 and 6, respectively. In contrast, no detectable bands were observed for bundle-CPSA/BMP implants in lanes 5 and 7.

Figure 10 shows the 2% agarose gel electrophoresis pattern of the mRNA expression of ball- and bundle-CPSA with rhBMP-2 at 4 weeks after implantation. Lane 1 is the standard. In lanes 2 and 3, GAPDH expression is observed as a bands in the 343 bp region for ball- and bundle-CPSA/BMP implants, respectively. Bands at 410 and 490 bp for the ball-CPSA/BMP implants indicate the expression of Flt-1 and KDR (lanes 4 and 6, respectively), whereas, no detectable Flt-1 and KDR bands are observed in case of bundle-CPSA/BMP in lanes 5 and 7. Flt-1 and KDR, two important receptors of VEGF, are expressed in the ball-CPSA/BMP implants but not in the bundle-CPSA/BMP at both 2 and 4 weeks after implantation.

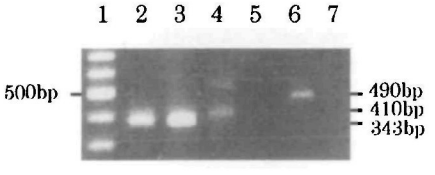

Fig. 9. **Photograph of 2% agarose electrophoresis gels showing the RT-PCR products of mRNA extracted from ball- and bundle-CPSA/BMP at 2 weeks after implantation and stained with ethidium bromide.** The GAPDH bands of ball- and bundle-CPSA/BMP samples appearing at the 343 bp sites are observed in lanes 2 and 3, respectively. Flt-1 and KDR bands of the ball-CPSA/BMP samples appear at the 410 and 490 bp sites in lanes 4 and 6, respectively. No detectable Flt-1 or KDR bands are seen for bundle-CPSA/BMP (lanes 5 and 7, respectively). The first lane on the left is a 100-bp marker ladder.

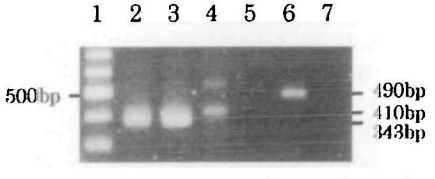

Fig. 10. **Photograph of 2% agarose electrophoresis gels showing RT-PCR products of mRNA extracted from 4-week ball- and bundle-CPSA/BMP stained with ethidium bromide.** The GAPDH bands of ball- and bundle-CPSA/BMP samples appearing at the 343 bp sites are observed in lanes 2 and 3, respectively. Flt-1 and KDR bands for the ball-CPSA/BMP samples appear at the 410 and 490 bp sites in lanes 4 and 6, respectively. No detectable Flt-1 or KDR bands are observed for bundle-CPSA/BMP (lanes 5 and 7, respectively). The first lane on the left is a 100-bp marker ladder.

DISCUSSION

Significance of CPSA as a Biomaterial—In this study, we attempted to use a novel material called CPSA glass fiber as a BMP-carrier, and proved that it works effectively if molded into a porous ball. The results were interpreted in terms of the "vasculature-inducing geometry" of the CPSA glass fibers. These results support the hypothesis that good vascularization and a suitable matrix scaffold are essential factors for bone formation.

The term "bioactive material" indicates "a material that elicits a specific biological response at the interface of the material, which results in the formation of a bond between the tissues and the materials" (Hench and Wilson, 1993). Many bioactive glasses have been introduced by different investigators. Bioglass® was first discovered by Hench and was shown to bond to both bone and soft tissues (*24*, *25*). Recently, Kokubo *et al.* developed A-W (apatite-wollastonite) glass by mixing hydroxyapatite with wollastonite (*26*). This new bioglass is characterized by its mechanically high strength and biocompatibility. Nakamura *et al.* (*27*) and Ijiri *et al.* (*28*) also confirmed these properties. More recently, Kobayashi *et al.* (*19*) invented another new bioglass, CPSA glass, in a fiber form. Morishita *et al.* (*19*) worked out the mechanical properties and biocompatibilities of CPSA fibers, which show a tensile strength of 2.10 GPa and Young modulus of 69.0 GPa. They implanted CPSA fibers into the bone marrow cavity of a rabbit femur for 6 weeks and showed that bone formation occurred in the area surrounding the CPSA fibers and that there was no tissue rejection. Thereafter, CPSA glass fibers were employed as a fiber-reinforced composite (FRC) for various clinical uses in the dental field, especially as aesthetic wire in orthodontic treatment combined with methyl methacrylate (*20*). We noticed that this is the only bioglass that can be molded into a fiber form. Thus, in this study, we fabricated geometrically different ball- and bundle-shaped structures and, combined with rhBMP-2, implanted them subcutaneously in rats.

Superiority of the Ball over the Bundle-Shape—The histological evidence showed clear-cut higher and faster cartilage and bone formation using the ball-CPSA/BMP rather than the bundle-CPSA/BMP (Fig. 4, A–D). One-week after implantation, the ball-CPSA/BMP showed chondrogenesis with the formation of hypertrophic chondrocytes (Fig. 3). More bone and marrow formation were observed for ball-CPSA/BMP than bundle-CPSA/BMP 2 weeks after implantation (Fig. 4, A and B). After 4 weeks, a very small amount of bone was observed around the bundle-CPSA/BMP, whereas the ball-CPSA/BMP showed large amounts of bone formation between the glass fibers with the formation of bone marrow spaces (Fig. 4, C and D). Lamellar bone with marked widening of the marrow spaces was also observed in the case of ball-CPSA/BMP at 20 weeks with no inflammatory reaction (Fig. 4E). Neither bone nor cartilage formation was observed for ball-CPSA without rhBMP-2, even 4 weeks after implantation (Fig. 4F).

Alkaline phosphatase (ALP) is a widely distributed glycosylated membrane-bound ectoenzyme. Bone ALP is located on the surface of osteoblasts and is thought to play a major role in bone formation and mineralization. Its levels are considered to reflect osteoblastic activity. Therefore, bone ALP levels can also be used as a biochemical marker for assessing bone related diseases, including bone metastasis (*29*). In our study, the ball-CPSA/BMP showed 10 times more ALP activity than bundles at the second week (Fig. 6). At the fourth week, the osteocalcin content of the ball-CPSA/BMP was 5 times higher than that of bundle-CPSA/BMP implants (Fig. 8). These results clearly indicate that the ball-CPSA/BMP is much more feasible for bone formation than bundle-CPSA/BMP.

Porosity of the BMP Carrier and Vasculature—Based on the five factors for bone formation described in the Introduction, there are two possible explanations for the differences between the ball- and bundle-CPSA/BMP. One is the efficacy of the migration of mesenchymal cells into the two carriers, and the other is vascularization into the carrier. The fundamental difference between the ball- and bundle-CPSA is their porosities. The ball-CPSA, with its diameter of 6 mm, has approximately 3 times as much vacant space as the bundle with a 3 mm diameter. It can easily be assumed that the higher porosity in the ball-CPSA will accept a much higher degree of mesenchymal cell migration and vascularization than in the bundle-CPSA. Vascular endothelial growth factor (VEGF) is a key regulator of vasculogenesis and angiogenesis that acts especially on endothelial cells, because VEGF receptors are expressed almost exclusively by the endothelium (*30*). As VEGF has the potency to increase vascular permeability, it has also been termed a vascular permeability factor (VPF). The fms-like tyrosine kinase (Flt-1) and kinase-domain-region (KDR) are the VEGF receptors (*31*, *32*). Both receptors share common features including seven Ig-like extracellular domains, a single transmembrane region, and a consensus tyrosine kinase sequence interrupted by a kinase insert domain. Their molecular masses are about 220 kDa, and they are highly glycosylated. Several studies have mapped the binding site for VEGF to the second Ig-like domains of Flt-1 and KDR, and deletion of the second Ig-like domain of Flt-1 completely abolishes VEGF binding (*33*, *34*). In our study, the results of the evaluation of vascular development by the RT-PCR study of Flt-1 and KDR receptor expression clearly indicated that the ball-CPSA/BMP shows strongly positive reactions at 2 and 4 weeks after implantation while the bundle-CPSA/BMP shows no detectable amounts at the same implantation periods (Figs. 9 and 10). These observations are consistent with the much higher osteogenesis for the ball-CPSA/BMP as judged by alkaline phosphatase activity, osteocalcin and histological observations.

It has been well documented that vascularization is an essential requirement for bone formation, but not for cartilage formation (*35*). However, little direct biochemical evidence for the correlation between osteogenesis and vasculature is available. To our knowledge, our report is the first to show a direct relationship between osteogenesis and vasculature.

Although the precise molecular mechanism of the differential requirements of osteoblasts and chondrocytes for vasculature is still not fully understood, this study provides positive evidence for the strong relationship between vasculature and osteogenesis in a BMP-induced ectopic system. Previously, several researchers have suggested possible mechanisms for the relationships among osteogenesis, vasculature, and matrices. One group emphasized vasculature as a source of osteoblasts (*36*); another group was inter-

ested in the higher oxygen and nutrient requirements of osteoblasts compared with chondrocytes (*37*, *38*). Recently, it was proposed that pericytes in the newly formed capillaries contribute to osteogenesis as a source of osteoblasts and signals for osteoblast recruitment in remodeling bone (*35*). Conclusive evidence is still lacking, although an, involvement of pericytes in supplying osteoblasts would indicate a stronger relationship between bone and vasculature.

Higher Oxygen Requirement of Osteoblasts—The higher oxygen and nutrient requirements of osteoblasts, were first proposed by Bassett (*37*). He showed that low oxygen tension (5%) favors chondrogenesis in organ cultures of chick embryo tibial cortex, while high oxygen tension (35%) favors bone formation. Reddi and Huggins (1973) showed that matrices of open and dead-end tube structures have different effects on osteogenesis and chondrogenesis inside the tubes (*39*). These two geometrically different forms were prepared using the middle and apical parts of rat incisor dentin for the open and dead-end tubes, respectively. The tubes were packed with decalcified bone particles and implanted into rat skin. The results showed that the open tubes induce osteogenesis and the dead-end tubes induce chondrogenesis. The authors interpreted the results by the higher vasculature in the open tube, suggesting that the higher supply of oxygen and nutrients in the open tubes favored osteogenesis while chondrogenesis was favored in dead-end tubes. Their report was also one of the first to describe the geometrical effect of the extracellular environment (*39*, *40*). Later, Sampath and Reddi (1984) reported that a coarse powder (particle size of 420–850 μm) of demineralized bone induces a much higher yield of bone than a fine powder (44–74 μm) when used as a carrier of BMP-induced bone formation (*41*).

Ripamonti and colleagues (1994) demonstrated the regulation of the geometrical factor of the substratum using porous hydroxyapatite (*42*) and monolithic discs of hydroxyapatite (*43*). However, the authors did not mention or verify vasculature as a causative factor in the differentiation between chondrogenesis and osteogenesis.

Vascular-Inducing Geometry—We have developed and tested more than ten BMP-carriers with different geometric properties, and have reached the conclusion that vasculature and bone formation are highly related to one another (*1*, *3*, *8*, *11*, *15–18*, *44*, *45*). Kuboki *et al.* (1995) demonstrated the effect of geometrical maxtrix factors in cell-differentiation using two distinctive BMP-carriers, fibrous glass membranes (FGM) and porous particles of hydroxyapatite (PPHAP), which induce zonal chondrogenesis and membranous ossification, respectively (*15*). The fibrous glass membrane (FGM), an unwoven sheet of glass fibers (fibril diameter, 1 μm; thickness, 1 mm), when combined with BMP and implanted into rat skin produces exclusively cartilage within the membrane. This result was explained by the finding that FGM prevents capillary invasion while allowing young mesenchymal cells to enter, proliferate and differentiate into chondrocytes (*15*). However, over a prolonged time, the network structure of FGM is gradually degraded except for the vascular development, and cartilage is replaced by bone (*18*). When the same glass fibers were molded into a ball, combined with BMP, and implanted onto rat skin, they did not induce the formation of cartilage or bone (data not shown). This was probably due to the small pore size within the ball that excluded both cellular migration and vasculature.

Recently, Takita *et al.* (*44*) showed that the same FGM combined with rhbFGF and rhBMP2 enhances osteogenesis at 2 weeks, while cartilage formation decreases, probably due to the increasing effect of bFGF on vascularization.

On the other hand, direct bone formation without chondrogenesis definitely occurred using the porous particles of hydroxyapatite (PPHAP) when combined with BMP as the carrier (*11*, *15*). This direct bone formation was explained by rapid vascularization through the interconnected pores in the PPHAP, which did not provide the hypoxic microenvironment necessary for chondrogenesis (*11*, *15*). Recently, Murata *et al.* (*45*) demonstrated the carrier dependency of cellular differentiation using porous particles of hydroxyapatite (PPHAP) combined with BMP and confirmed that the PPHAP/BMP composite induces only direct bone formation without chondrogenesis. Sasano *et al.* (*16*) also showed direct bone formation in the local area within the carrier, independent of endochondral ossification, using a fibrous collagen membrane (FCM) with BMP. Kuboki *et al.* (*11*) compared three hydroxyapatite ceramics with different geometrical structures for their efficacies as carriers for BMP-induced osteogenesis: solid non-porous particles, coral- replicated porous discs of hydroxyapatite (5 mm in diameter and 2 mm in height, a gift from Interpore International, Irvine, USA), and PPHAP were subcutaneously implanted into rats. The results indicated that PPHAP and coral-HAP induced osteogenesis effectively due to the geometry of the interconnected porous structures that creates spaces for vasculature. On the other hand, solid non-porous particles did not induce osteogenesis or chondrogenesis because the smooth structure and close contact of the particles inhibits vascular formation and the proliferation of mesenchymal cells. They proposed that a feasible geometry of hydroxyapatite for osteogenesis is an interconnected porosity that leads to vascularization.

Tsuruga *et al.* (*3*), using a carrier geometrically different but composed of the same material, demonstrated that the most favorable pore size in the porous hydroxyapatite block (PBHAP) combined with BMP for osteogenesis is 300–400 μm. Interestingly, the Haversian system in bone remodeling (approximately 300 μm in diameter) coincides with the optimal size of the same material.

Vasculature-Inducing Geometry of CPSA—The carrier-dependent osteogenesis and chondrogenesis in the above reports may be attributed to the high oxygen tension and nutrients provided by the increased vascularization in the feasible geometry, which favors osteogenesis, whereas, low oxygen tension favors chondrogenesis, a fact verified by Bassett and Herrmann (*46*). Thus, we propose that as a general rule: BMP, if combined with a carrier in which vascular invasion is geometrically feasible, can induce immature cells to become bone-forming cells that cause the direct formation of bone. On the other hand, BMP combined with a carrier for which vascular invasion is geometrically less feasible first induces cartilage, which eventually leads to bone formation as the capillaries grow. Thus, the porous structure is crucially important for vascularization.

More recently, a new BMP carrier, a honeycomb-shaped hydroxyapatite (HCHAP), confirmed the idea of tubing geometry for vascularization (*47*). This BMP-carrier contains 7 tunnels, each 110 μm in diameter and about 1.5 mm length, in which the biomimetic process of endochondral

ossification was observed.

Unlike with other hydroxyapatite BMP-carriers, cartilage first filled the space within the tunnel. Then, the cartilage was replaced by vascular invasion along with bone formation on the inner surfaces of the tunnels. This was considered to be due to the delay of vascular development throughout the extremely long length of the tunnel (*47*). The results further confirm the above conclusion that the geometry of the BMP-carrier controls the differentiation into chondrogenesis and osteogenesis.

The ball-CPSA/BMP in the present paper, due to its porous structure, is favorable for the invasion of cells and blood capillaries in implants, leading to more bone formation than in the case of bundle-CPSA/BMP. This vasculature-inducing geometry may also favor the phenotypic expression of bone cells as a cell substratum. However, since the spaces created by fibrous material are relatively heterogenous in nature, it is assumed that there will be many local sites lacking vascular development, allowing cartilage formation until the second week after implantation.

From the above observations, "vasculature-inducing geometry" is defined as the optimal porous scaffold of the implant material in either solid or fiber form that functions as cell substrata, provides spaces and guides for vascular capillary invasion, and affects cell growth and differentiation leading to a certain phenotypic expression of cells to grow into tissues. The concept of "vasculature-inducing geometry" of the BMP-carrier proposed here may be applicable to tissue-engineering techniques in advanced clinical treatment, and more efficient cell cultures, particularly for bone and cartilage cells. A scaffold with a vasculature-inducing geometry is indispensable if the cells are to grow into tissues larger than a certain size. A simple and clear example of a feasible geometric form composed of fibrous biomaterial is presented in this paper.

Vascularization as a New Marker for Bone Formation—Also in this paper, to correlate osteogenesis with vascularization, we analyzed the mRNA expression of important specific receptors of VEGF, Flt-1, and KDR, in the two geometrically different scaffolds, ball- and bundle-CPSA/BMP, in an ectopic model system. The results showed that Flt-1 and KDR are distinctly expressed in ball-CPSA/BMP at 2 and 4 weeks after implantation (Figs. 9 and 10). In contrast, no expression was detectable in the bundle-CPSA/BMP at the same post implantation times, indicating a clear relationship between higher neovascularization and osteogenesis in the porous CPSA balls. To our knowledge, this is the first demonstration of the relationship between mRNA of vasculature-related proteins and active osteogenesis. Thus, the expression of these mRNAs or proteins can be used as a new marker of osteogenesis.

REFERENCES

1. Kuboki, Y., Yamaguchi, H., Yokoyama, A., Murata, M., Takita, H., Tazaki, M., Mizuno, M., Hasegawa, T., Iida, S., Shigenobu, K., Fujisawa, R., Kawamura, M., Atuta, T., Matumoto, A., Kato, H., Zhou, H-Y, Ono, I., Takeshita, N., and Nagai, N. (1991) *The Bone-Biomaterial Interface. Osteogensis Induced by BMP-Coated Biomaterials: Biochemical Principles of Bone Reconstruction in Dentistry*, pp. 127–138, University Toronto Press, Toronto
2. Kuboki, Y., Sasaki, M., Saito, A., Takita, H., and Kato, H. (1998) Regeneration of periodontal ligament and cementum by BMP-applied tissue engineering. *Eur. J. Oral Sci.* **106**, 197–203
3. Tsuruga, E., Takita, H., Itoh, H., Wakisaka, Y., and Kuboki, Y. (1997) Pore size of porous hydroxyapatite as the cell-substratum controls BMP-induced osteogenesis. *J. Biochem.* **121**, 317–324
4. Fujisawa, R., Nodasaka, Y., and Kuboki, Y. (1995) Further characterization of interaction between bone sialoprotein (BSP) and collagen. *Calcif. Tissue Int.* **56**, 140–144
5. Mizuno, M. and Kuboki, Y. (1995) TGF-beta accelerated the osteogenic differentiation of bone marrow cells induced by collagen matrix. *Biochem. Biophys. Res. Commun.* **211**, 1091–1098
6. Takita, H. and Kuboki, Y. (1995) Conformational changes of bovine bone osteonectin induced by interaction with calcium. *Calcif. Tissue Int.* **56**, 559–565
7. Fujisawa, R., Mizuno, M., Nodasaka, Y., and Kuboki, Y. (1997) Attachment of osteoblastic cells to hydroxyapatite crystals by a synthetic peptide (Glu7-Pro-Arg-Gly-Asp-Thr) containing two functional sequences of bone sialoprotein. *Matrix Biol.* **16**, 21–28
8. Kuboki, Y., Takita, H., Komori, T., Mizuno, M., Furu-uchi, E., and Taniguchi, K. (1989) Seperation of bone matrix proteins by calcium-induced precipitation. *Calcif. Tissue Int.* **44**, 269–277
9. Kuboki, Y., Okuguchi, M., Takita, H., Kimura, M., Tsuzaki, M., Takakura, A., Tsunazawa, S., Sakiyama, F., and Hirano, H. (1993) Amino-terminal location of pyridinoline in dentin collagen. *Connect. Tissue Res.* **29**, 99–110
10. Tucker, A S., Matthews, K.L., and Sharpe, P.T (1998) Transformation of tooth type induced by inhibition of BMP signaling. *Science* **282**, 1136–1138
11. Kuboki, Y., Takita, H., Kobayashi, D., Tsuruga, E., Inoue, M., Murata, M., Nagai, N., Dohi, Y., and Ohgushi, H. (1998) BMP-induced osteogenesis on the surface of hydroxyapatite with geometrically feasible and non feasible structures: Topology of osteogenesis. *J. Biomed. Mater. Res* **39**, 190–199
12. Reddi, A.H. (1981) Cell biology and biochemistry of endochondral bone development. *Coll. Res.* **1**, 209–226
13. Urist, M.R. (1965) Bone formation by autoinduction. *Science* **150**, 893–899
14. Wozney, J.M., Rosen, V., Celeste, A.J., Mitsock, L.M., Whitters, M.J., Kriz, R.W., Hewick, R.M., and Wang, E.A. (1988) Novel regulators of bone formation: Molecular clones and activities. *Science* **242**, 1528–1534
15. Kuboki, Y., Saito, T., Murata, M., Takita, H., Mizuno, M., Inoue, M., Nagai, N., and Poole, A.R. (1995) Two distinctive BMP carriers induce zonal chondrogenesis and membranous ossification, respectively: Geometrical factor of matrices for cell differentiation. *Connect. Tissue Res.* **32**, 219–226
16. Sasano, Y., Ohtani, E., Narita, K., Kagayama, M., Murata, M., Saito, T., Shigenobu, K., Takita, H., Mizuno, M., and Kuboki, Y. (1993) BMPs induce direct bone formation in ectopic sites independent of the endochondral ossification in vivo. *Anat. Rec.* **236**, 373–380
17. Kuboki, Y., Takita, H., Tsuruga, E., Ono, M., and Jansen, J.A. (1998) Rationale for hydroxyapatite-coated titanium-mesh as an effective carrier for BMP. *Dent. Res.* **77(A)**, 263
18. Sasano, Y., Mizoguchi, I., Takahashi, I., Kagayama, M., Saito, T., and Kuboki, Y. (1997) BMPs induce endochondral ossification in rats when implanted ectopically within a carrier made of fibrous glass membrane. *Anat. Rec.* **247**, 472–478
19. Morishita, M., Kobayashi, M., Seyama, M., Kondo, S., Kawaguchi, K., Arai, H., Tagai, H., and Kuroki, Y. (1987) Mechanical properties and biocompatibilities of the new glass-fiber composite materials as artificial bone in *Biomaterials and Clinical Applications*, pp. 275–280, Elsevier science publishers B.V., Amsterdam
20. Imai, T., Watari, F., Yamagata, Kobayashi, M., Nagayama, K., Toyoizumi, Y., and Nakamura, S. (1998) Mechanical properties and aesthetics of FRP orthodontic wire fabricated by hot drawing. *Biomaterials* **19**, 2195–2200
21. Kind, P.R.N. and King, E.J. (1954) Estimation of plasma phosphate by determination of hydrolizes phenol with amino-antipyrine. *J. Clin. Pathol.* **7**, 322–326
22. Bilbe, G., Robers, E., Birch, M., and Evans, D.B. (1996) PCR

phenotyping of cytokines, growth factors and their receptors and bone matrix proteins in human osteoblast-like cell line. *Bone* **19**, 437–445
23. Yeh, L-C.C. and Lee, J.C. (1999) Osteogenic protein-1 increases gene expression of vascular endothelial growth factor in primary cultures of fetal rat calvaria cells. *Mol. Cell. Endocrinol.* **153**, 113–124
24. Hench, L.L. and Paschall, H.A. (1973) Direct chemical bond of bioactive glass-ceramic materials to bone and muscle. *J. Bimed. Mater. Res. Symp.* **4**, 25–42
25. Hench, L.L. and Wilson, J. (1984) Surface-active biomaterials. *Science* **226**, 630–636
26. Kokubo, T., Kushitani, H., Sakka, S., Kitsugi, T., and Yamamuro, T. (1990) Solutions able to reproduce in vivo surface-structure changes in bioactive glass-ceramic A-W^3. *J. Biomed. Mater. Res.* **24**, 721–734
27. Nakamura, T., Yamamuro, T., and Higashi, S. (1985) A new glass-ceramic for bone replacement: Evaluation of its bonding to bone tissue. *J. Biomed. Mater Res.* **19**, 685–698
28. Ijiri, S., Nakamura, T., Fujisawa, Y., Hazama, M., and Komatsudani, S. (1997) Ectopic bone induction in porous apatite-wollastonite-containing glass-ceramic combined with bone morphogenetic protein. *J. Biomed. Mater. Res.* **35**, 421–431
29. Nakayama, M., Gorai, I., Minaguchi, H., Rosenquist, C., and Qvist, P. (1998) Purification and characterization of bone-specific alkaline phosphatase from a human osteosarcoma cell line. *Calcif. Tissue Int.* **62**, 67–73
30. Risau, W. (1997) Mechanisms of angiogenesis. *Nature* **386**, 671–674
31. Olofsson, B., Korpelainen, E., Pepper, M.S., Mandriota, S.J., Aase, K., Kumar, V., Gunji, Y., Jeltsch, M.M., Shibuya, M., Alitalo, K., and Eriksson, U. (1998) Vascular endothelial growth factor B (VEGF-B) binds to VEGF receptor-1 and regulates plasminogen activator activity in endothelial cells. *Proc. Natl. Acad. Sci. USA* **95** (20), 11709–11714
32. Achen, M.G., Jeltsch, M., Kukk, E., Makinen, T., Vitali, A., Wilks, A.F., Alitalo, K., and Stacker, S.A.. (1998) Vascular endothelial growth factor D (VEGF-D) is a ligand for the tyrosine kinases VEGF receptor 2 (Flk-1) and VEGF receptor 3 (Flt 4). *Proc. Natl. Acad. Sci. USA* **95**, 548–553
33. Davis-Smyth, T., Chen, H., Park, J., Presta, L.G., and Ferrara, N. (1996) The second immunoglobulin-like domain of the VEGF tyrosine kinase receptor Flt-1 determines ligand binding and may initiate a signal transduction cascade. *EMBO J.* **15**, 4919–4927
34. Berleon, B., Totzke, F., Herzog, C., Blanke, S., Kremmer, E., Siemeister, G., Marme, D., and Martiny-Baron, G. (1997) Mapping of the sites for ligand binding and receptor dimerization at the extracellular domain of the vascular endothelial growth factor FLT-1. *J. Biol. Chem.* **272**, 10382–10388
35. Parfitt, A.M. (2000) The mechanism of coupling: A role for the vasculature. *Bone* **26**, 319–232
36. Trueta, J. (1963) The role of the vessels in osteogenesis. *J. Bone Joint Surg.* **45B**, 402–418
37. Bassett, C.A.L. (1962) Current concepts of bone formation. *J. Bone Joint Surg.* **44A**, 1217–1244
38. Reilly, T.M., Seldes, R., Luchetti, W., and Brighton, C.T. (1998) Similarities in the phenotypic expression of pericytes and bone cells. *Clin. Orthop.* **346**, 95–103
39. Reddi, A.H. and Huggins, C.B. (1973) Influence of geometry of transplanted tooth and bone on transformation of fibroblasts. *Proc. Soc. Exp. Biol. Med.* **143**, 634–637
40. Sampath, T.K. and Reddi, A.H. (1981) Dissociative extraction and reconstruction of extracellular matrix components involved in local bone differentiation. *Proc. Natl. Acad. Sci. USA* **78**, 7599–7603
41. Sampath T.K. and Reddi A.H. (1984) Importance of geometry of the extracellular matrix in endochondral bone differentiation *J. Cell Biol.* **98**, 2192–2197
42. Van Eeden, S.P. and Ripamonti, U. (1994) Bone differentiation in porous hydroxyapatite in baboons is regulated by the geometry of the substratum: Implications for reconstructive craniofacial surgery. *Plas. Reconstr. Surg.* **93**, 959–966
43. Ripamonti, U., Crooks, J., and Kirkbride, A.N. (1999) Sintered porous hydroxyapatites with intrinsic osteoinductive activity: geometric induction of bone formation. *S. Afr. J. Sci.* **95**, 335–343
44. Takita, H., Tsuruga, E., Ono, I., and Kuboki, Y. (1997) Enhancement by bFGF of osteogenesis induced by rhBMP-2 in rats. *Eur. J. Oral Sci.* **105**, 588–592
45. Murata, M., Inoue, M., Arisue, Kuboki, Y., and Nagai, N. (1998) Carrier- dependency of cellular differentiation induced by bone morphogenetic protein in ectopic sites. *Int. J. Oral Maxillofac. Surg.* **27**, 391–396
46. Bassett, C.A.L. and Herrmann, I. (1961) Influence of oxygen concentration and mechanical factors on differentiation of connective tissues in vitro. *Nature* **190**, 460–461
47. Jin, Q.-M., Takita, H., Kohgo, T., Atsumi, K., Itoh, H., and Kuboki, Y. (2000) Effects of geometry of hydroxyapatite as a cell substratum in BMP-induced ectopic bone formation. *J. Biomed. Mater. Res.* **51**, 491–499